PAPER • OPEN ACCESS
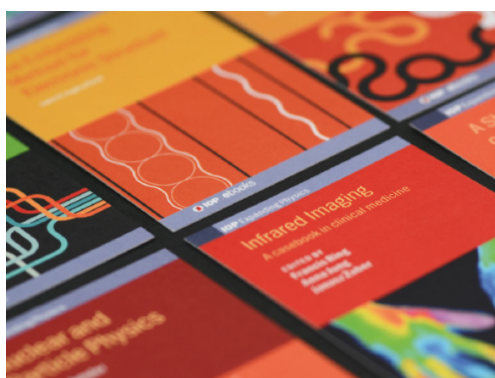
Electromagnetically induced transparency in a V-system with ^{87}Rb vapour in the hyperfine Paschen-Back regime

View the article online for updates and enhancements.

Electromagnetically induced transparency in a V-system with ^{87}Rb vapour in the hyperfine Paschen-Back regime

Clare R Higgins[*] and **Ifan G Hughes**

Department of Physics, Durham University, South Road, Durham, DH1 3LE, United Kingdom

E-mail: clare.r.higgins@durham.ac.uk

CrossMark

Abstract
We observe electromagnetically induced transparency (EIT) in a V-system in a thermal rubidium-87 vapour in the hyperfine Paschen-Back regime, realised with a 0.6 T axial magnetic field. In this regime energy levels are no longer degenerate and EIT features from different initial states are distinct, which we show produces a much cleaner feature than without a magnetic field. We compare our results to a model using the time-dependent Lindblad master equation, and having averaged over a distribution of interaction times, see good qualitative agreement for a range of pump Rabi frequencies. Excited state decay into both ground states is shown to play a prominent role in the generation of the transparency feature, which arises mainly due to transfer of population into the ground state not coupled by the probe beam. We use the model to investigate the importance of coherence in this feature, showing that its contribution is more significant at smaller pump Rabi frequencies.

Keywords: V-systems, ^{87}Rb, thermal vapours, electomagnetically induced transparency

(Some figures may appear in colour only in the online journal)

1. Introduction

Electromagnetically induced transparency (EIT) is an optical phenomenon involving three quantum states coupled by two optical fields (laser beams). In an absorbing medium, a transparency window in the transmission of a weak probe beam on one transition is induced by the presence of a strong pump beam on another transition [1]. Throughout the text we refer to these beams as 'pump' and 'probe'. EIT has been widely studied and has potential applications in precision magnetometers [2–4], slow light generation [5, 6], quantum information [7, 8], and atomic clocks [9]. There are three possible configurations of EIT: V; lambda; and ladder [10]. V-EIT is the least studied of these because there is no stable dark state [11], as both of the singly coupled states are excited states and can decay to the ground state. Nevertheless, V-EIT has been extensively studied [6, 12–25], and provides an interesting testing ground for ascertaining the relative importance of coherent and incoherent mechanisms in the generation of the transparency window [16, 26, 27].

One of the main obstacles to overcome in modelling and understanding V-EIT in thermal vapours is the complexity introduced by the overlapping spectral lines, as a consequence of the degeneracies of the magnetic sub-levels and the excited-state hyperfine splitting being less than the Doppler width of the probed transition. To circumvent these difficulties, we use the hyperfine Pashen-Back regime [28–35] where the energy levels are non-degenerate. A 0.6 T magnetic field used with ^{87}Rb vapour on the D1 and D2 lines leads to isolated transitions separated by more than their Doppler width. Previous work has shown that operating in this regime allows simplified energy-level schemes and theoretical models, leading to good agreement between theory and experiment [36–39].
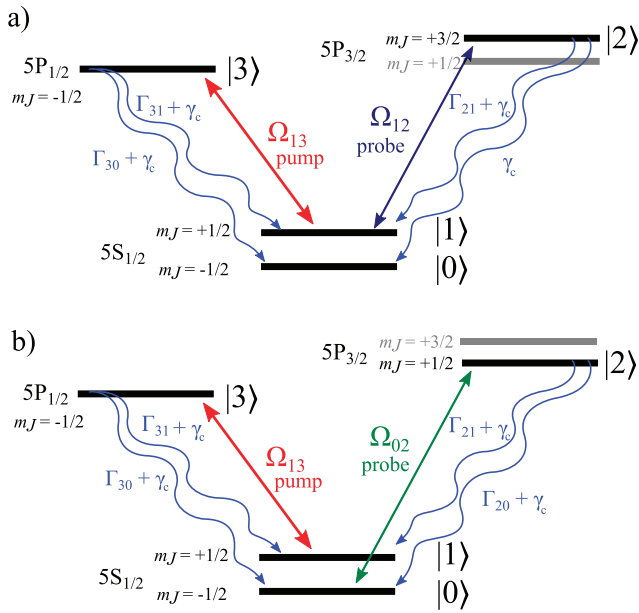
Figure 1. The energy levels involved in our system. (a) Shows the EIT configuration, in which the 780 nm probe beam is coupling $m_J = +1/2$ to $m_J = +3/2$. In (b) the probe beam is instead tuned to couple the $m_J = -1/2$ to $m_J = +1/2$ transition, which excites out of $|0\rangle$, the non-pump-coupled ground state. This configuration does not produce EIT, but demonstrates that population moves from $|1\rangle$ to $|0\rangle$. These two probe positions produce the set 1 and set 2 of peaks in figure 5, respectively. Ω_{ab} are the driving Rabi frequencies, between initial state a and final state b. The decays between states have two contributions: Γ_{ab}, the natural linewidth, and γ_c, the collisional decay to each ground state. The probe (pump) is left (right)-hand circularly polarised and couples σ_+ (σ_-) transitions [40].

2. Theory

Our V-EIT system, realised in the hyperfine Paschen-Back regime, is shown in figure 1(a). The levels we use, marked $|1\rangle$, $|2\rangle$ and $|3\rangle$, do not form a closed system. We use 'closed system' to mean the atoms do not decay to any states outside of the three EIT levels, and 'open system' when decay to other, non laser-coupled states, is possible. The pumped transition—from $|1\rangle$ to $|3\rangle$—is an open transition so $|3\rangle$ can decay to the other, uncoupled, ground state. This adds a fourth level into the system, which we label $|0\rangle$. The pump causes population transfer from $|1\rangle$ to $|0\rangle$, resulting in reduced absorption of the probe which couples $|1\rangle$ and $|2\rangle$. The driving Rabi frequencies are labelled Ω_{ab}, where a and b represent the initial and final states respectively. The decays between states have two contributions: the natural linewidth, Γ_{ab}, and a collisional decay to each ground state, γ_c. The second is present even where dipole-allowed transitions are forbidden, and the total collisional decay from an excited state has been experimentally determined in this vapour cell as $2\gamma_c/2\pi = 7$ MHz [36]. The natural linewidths (linear) of states $|2\rangle$ and $|3\rangle$ are 6.0 MHz and 5.7 MHz, respectively. These are split along the two decay paths according to the branching ratios calculated using Wigner 3-j symbols. Part (b) shows the state configuration when the probe is instead tuned to the transition between $|0\rangle$ and $|2\rangle$. This is not an EIT setup, but allows us to see the enhanced absorption caused by the extra population in $|0\rangle$.
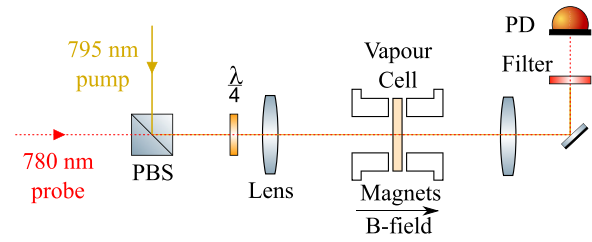

Figure 2. Experimental setup. Orthogonally linearly polarised 795 nm pump and 780 nm probe beams are combined on a polarising beam splitter (PBS) cube, and passed through a quarter waveplate converting them to right- and left-handed circularly polarised light, respectively. The beams are focussed through a 2 mm vapour cell in a longitudinal 0.6 T magnetic field, to an average beam waist of (83 ± 5) μm. The light transmitted through the cell passes through an interference filter to remove pump light, and is recorded on a photodiode (PD).

3. Experimental details

The experimental setup is shown in figure 2. We use a 2 mm long 98% ^{87}Rb vapour cell in a magnetic field, parallel to the laser propagation direction, of 0.6 T, produced by two cylindrical 'top hat' magnets. The orthogonally linearly polarised 795 nm and 780 nm beams are combined on a polarising beam splitter (PBS). A quarter waveplate transforms the polarisation to left-hand circular and right-hand circular respectively. A lens of focal length 200 mm focusses the beams to waists of (100 ± 5) μm × (78 ± 5) μm (780 nm) and (65 ± 5) μm × (90 ± 5) μm (795 nm) inside the cell. We aim to overlap the beams as completely as possible inside the cell by optimising the EIT feature, however due to the slight shape difference a perfect overlap is not possible. After the cell an interference filter removes pump light, and the probe transmission spectrum is measured on a photodiode (PD). We have a strong, resonant 795 nm pump, and a weak 780 nm scanning probe. We use a vapour temperature of 80 °C; at lower temperatures the signals are smaller, and at higher temperatures the absorption saturates and the features are distorted.

4. Experimental results

Figure 3 shows the advantage gained by using the hyperfine Paschen-Back regime. The top panels show theoretical D2 line spectra without a magnetic field (red) and with a 0.6 T field (blue). The two peaks used in the lower panels are shown highlighted. In the lower panels dotted lines are probe beam only; solid lines are when the pump beam is introduced. The probe only features have a Voigt profile with FWHM of ~550 MHz at 80 °C. The profile is dominated by its Gaussian component, which is due to the Doppler effect; atoms at finite temperature travel at a range of velocities which each absorb at a frequency displaced from resonance, given by $\omega = \omega_0 + kv$. Here ω is angular frequency, ω_0 is resonance angular frequency, k is wavenumber and v is the velocity component along the direction of propagation of the laser beams. The left panel shows experimental EIT features with no magnetic field, which shows contributions from several transitions. The right

J. Phys. B: At. Mol. Opt. Phys. **54** (2021) 165403
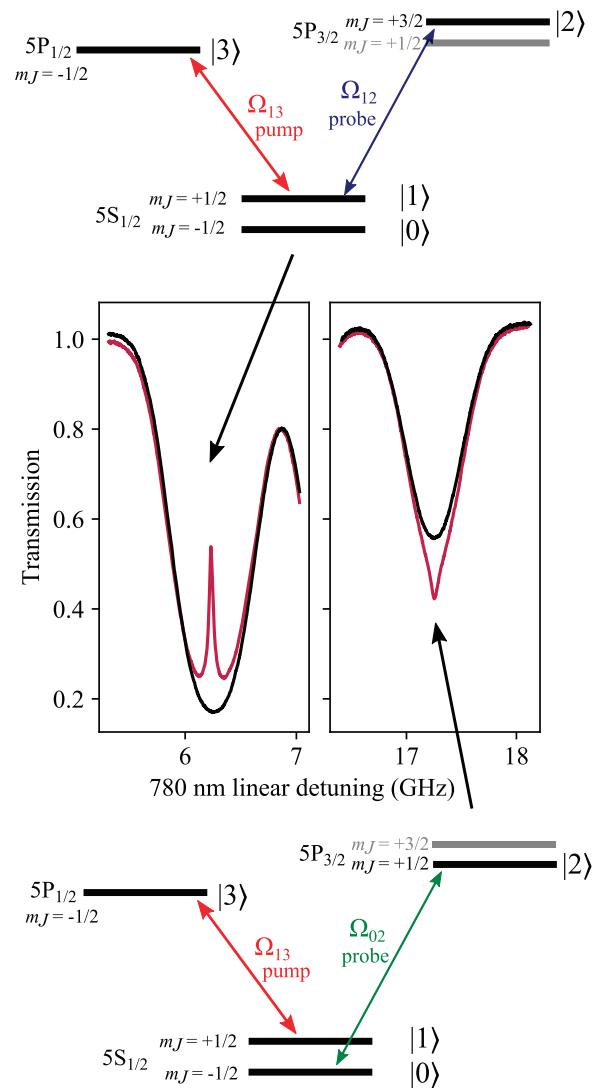
C R Higgins and I G Hughes
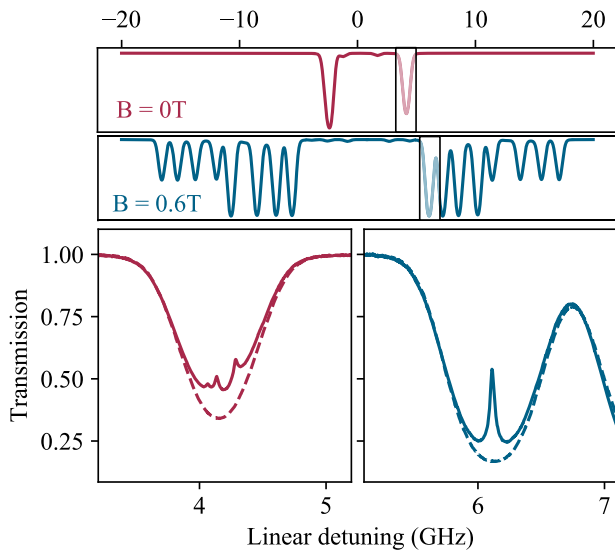
Figure 3. Upper panels: theoretical scans over D2 features without magnetic field (top, red), and with 0.6 T magnetic field (second panel, blue). Shaded rectangles show where the experimental spectra in the lower panels fit in the spectra. In the lower panels dotted lines are probe beam only, solid lines are when the pump beam is introduced. Left: experimental V-EIT feature with no magnetic field. Many hyperfine sublevels contribute producing a messy feature. Right: experimental feature in 0.6 T magnetic field. Energy levels are separated by more than the Doppler width so a single clean feature is seen.

Figure 4. Figure shows a 0.1 μW, 780 nm probe beam scan over the two $m_I = 3/2$ D2 transition lines at 0.6 T. The black trace is probe only, while the red traces shows the effect of introducing a 20 μW pump beam on the transition $|1\rangle \leftrightarrow |3\rangle$, as shown in the energy level diagrams. The energy level diagrams show which states the pump beam is coupling for the two features in the scan. Where the probe couples out of $|1\rangle$, there is a transparency feature, and where it couples out of $|0\rangle$ there is an enhanced absorption feature.

shows the feature in a 0.6 T field, where one clean feature is visible. Both features are produced in the same cell, with the same laser powers.

Figure 4 shows a scan over the two $m_I = 3/2$ D2 σ_+ absorption lines in a 0.6 T magnetic field. The black trace is a probe only scan, and the red traces shows the effect of adding in a 20 μW pump beam. Here, and throughout, we use a probe power of 0.1 μW. All the optical power values reported throughout this work are measured before the vapour cell, and have an error of $\pm 5\%$. We see that two different features appear; on the $m_J = -1/2 \rightarrow m_J = +1/2$ peak (left) we see a narrow transmission feature, characteristic of EIT. The states coupled at this point in the scan are shown in the diagram above. Notably the probe is coupling out of $|1\rangle$, the upper ground state. On the $m_J = -1/2 \rightarrow m_J = +1/2$ peak (right) there is an enhanced absorption feature. In this case, as shown in the lower diagram, the probe couples out of $|0\rangle$, the lower ground state. This state is populated by spontaneous decay from $|3\rangle$, which is itself populated by the strong pump beam.

Following on from figures 4 and 5 shows the effect of tuning the pump beam to different m_I transitions. The black trace in (a) shows a scan of the 780 nm probe over the D2 absorption lines at 0.6 T, with no pump. At 0.6 T, m_I and m_J are good quantum numbers. For ^{87}Rb, $I = 3/2$, therefore there are four possible values for m_I. The spectrum shows two sets of four transitions; in set 1(set 2) all four transitions are between states with initial $m_J = +1/2(-1/2)$ and final $m_J = +3/2(+1/2)$. Inside each set, each transition has a different m_I value, as labelled in the figure. The four coloured traces show the probe transmission when the pump is tuned to the correspondingly

coloured transition in (b). It is evident that when the pump is coupled to a particular m_I level in the upper ground state, $|1\rangle$, there is a transmission window in the probe absorption peak coupling out of that level (set 1 transitions). There is also a corresponding enhanced-absorption feature when the probe instead couples out of the lower ground state with the same m_I value, $|0\rangle$ (set 2 transitions). The EIT features shown in figure 5 have an FWHM of (39 ± 3) MHz.

5. Model

Atomic systems can be modelled using the Lindblad-master equation [10],

$$\frac{d\rho}{dt} = -\frac{i}{\hbar}[H, \rho] + L, \qquad (1)$$
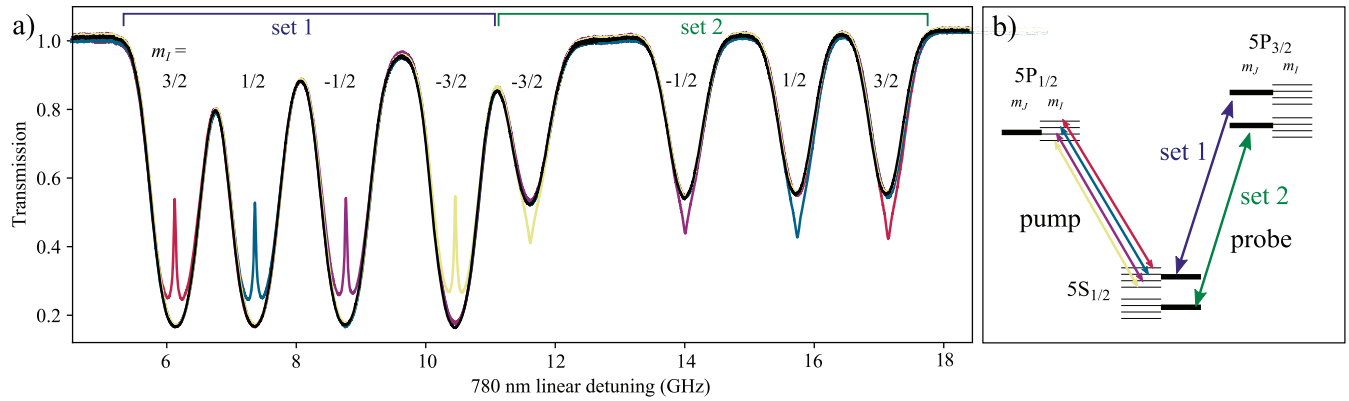
Figure 5. (a) Shows a 0.1 μW, 780 nm probe beam scan over the D2 transition lines at 0.6 T. The black trace is probe only, while the four coloured traces show the effect of introducing a 20 μW pump beam on the correspondingly coloured transition shown in (b). Each of the four pump transitions has a different m_I value. Introducing a particular m_I pump transition induces a transparency in the peak in set 1, and an enhanced absorption feature in the corresponding peak in set 2, which have the same m_I.

which describes the evolution of the density matrix, ρ,

$$\rho = \begin{pmatrix} \rho_{00} & \rho_{10} & \rho_{20} & \rho_{30} \\ \rho_{01} & \rho_{11} & \rho_{21} & \rho_{31} \\ \rho_{02} & \rho_{12} & \rho_{22} & \rho_{32} \\ \rho_{03} & \rho_{13} & \rho_{23} & \rho_{33} \end{pmatrix}, \qquad (2)$$

of the system. The diagonal elements, ρ_{aa}, are the population in each state, and the off-diagonal elements, ρ_{ab}, are the coherences between states. The system Hamiltonian, H, in the rotating wave approximation, has state detunings, Δ_{ab}, on the diagonals, and Rabi frequencies, Ω_{ab}, coupling the states on the off-diagonals. The Hamiltonian corresponding to the system in figure 1(a) is

$$H = \frac{\hbar}{2} \begin{pmatrix} 0 & 0 & 0 & 0 \\ 0 & 0 & \Omega_{12} & \Omega_{13} \\ 0 & \Omega_{12} & -2\Delta_{12} & 0 \\ 0 & \Omega_{13} & 0 & -2\Delta_{13} \end{pmatrix}, \qquad (3)$$

while the Hamiltonian for figure 1(b) is

$$H = \frac{\hbar}{2} \begin{pmatrix} 0 & 0 & \Omega_{02} & 0 \\ 0 & 0 & 0 & \Omega_{13} \\ \Omega_{02} & 0 & -2\Delta_{02} & 0 \\ 0 & \Omega_{13} & 0 & -2\Delta_{13} \end{pmatrix}. \qquad (4)$$

As we use a V system in a co-propagating geometry, we incorporate the Doppler effect into the model by setting $\Delta_{\text{pump}} \rightarrow \Delta_{\text{pump}} - k_{\text{pump}}v$ and $\Delta_{\text{probe}} \rightarrow \Delta_{\text{probe}} - k_{\text{probe}}v$. Prominent EIT features are observed with velocity groups where the residual two-photon doppler broadening ($k_{\text{pump}} - k_{\text{probe}})v < \Omega_{\text{pump}}$ [27]. This geometry makes the system Doppler insensitive, because the two photon resonance condition is maintained for atoms of non-zero velocity.

Decays between states are included in the Lindblad dissipator term, L, given by

$$L = \sum_n \frac{1}{2}[2C_n\rho C_n^{\dagger} - (\rho C_n^{\dagger}C_n + C_n C_n^{\dagger}\rho)], \qquad (5)$$

which is a sum over all decay modes, n, where $C_n = \sqrt{\gamma_n}A_n$ are collapse operators and A_n are operators which couple the

environment to the system with rate γ_n. For our system this means $C_{ab} = \sqrt{\Gamma_{ab} + \gamma_c}|b\rangle\langle a|$.

We solve the Lindblad master equation numerically for our four-level system. We model with a probe beam Rabi frequency of 0.96 MHz on the $m_J = +1/2 \rightarrow m_J = +3/2$, and, due to the differing dipole matrix elements of the transitions, a Rabi frequency of 0.55 MHz on the $m_J = -1/2 \rightarrow m_J = +1/2$ transitions. This puts us in the weak probe regime. We use a range of pump Rabi frequencies to produce a range of features which span those seen experimentally. This range is 2 MHz–100 MHz. The pumping transition we use is open, as the excited state, $|3\rangle$, can decay to both m_J ground states, $|0\rangle$ and $|1\rangle$, as depicted in figure 1(a). The pump and probe only couple to $|1\rangle$ so in the steady-state solution all the population ends up in the uncoupled ground state, $|0\rangle$, resulting in no absorption. We therefore have to use the time-dependent solutions. We have beams with an average $1/e^2$ radius of (83 ± 5) μm, from which we calculate the in-beam time-of-flight distribution, using the transverse velocity distribution [41–43]. For a given probe detuning the solutions are summed over all longitudinal velocity contributions [44]. The absorption profile is calculated from the imaginary part of the relevant coherence, which is a suitably weighted average of the result at each time step, and we use the Elecsus code [45] to calculate the linestrengths.

6. Comparison with experiment

Figure 6 shows the effect of changing pump power/Rabi frequency on the transmission and absorption features, with experimental results in the upper panels and model predictions in the lower panels. Optical power is related to Rabi frequency by the area of the beam and the dipole matrix element of the transition. Here, as we are not plotting theory and experiment on the same axis we use optical power for experiment, and Rabi frequency for theory. We see good qualitative agreement, with both the narrow transmission and the extra absorption feature correctly predicted, though the features are slightly narrower in theory than in experiment. We attribute the
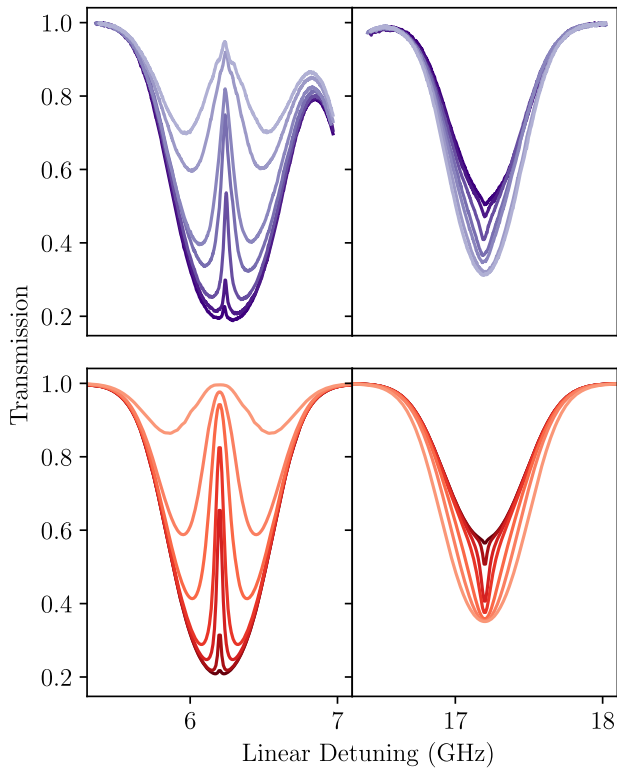
**Figure 6.** The effect of changing the 795 nm pump power on the induced transparency and enhanced absorption features on the $m_I = +3/2$ transitions of the D2 (780 nm, 0.1 μW) spectrum. Upper: experimental transmission spectra with changing pump powers, with values of in μW of 1 (dark), 5, 10, 50, 100, 500, 1000 (light). These correspond to Rabi frequencies in the range 2 MHz–100 MHz. The EIT features shown in the top left panel have FWHM ranging from (21 ± 3) MHz (lowest pump power) to (247 ± 5) MHz (highest pump power). Lower: modelled transmission spectra with pump Rabi frequencies in MHz of 1 (dark), 3, 10, 20, 50, 100, 300 (light). The range of Rabi frequencies was chosen to straddle the range of features seen in the experimental data; they are not calculated equivalents.

Figure 7. A comparison of experimental and modelled results. Black dashed line is experimental with 10 μW pump, which converts to an average linear Rabi frequency in the beam of 15 MHz. Two theory traces are plotted, chosen to fit the tip of the transparency feature (red) and the bottom of the absorption feature (blue). They have linear Rabi frequencies of 5.5 MHz and 12.0 MHz respectively, which are close to our experimental value. It is clear that for this model a pump Rabi-frequency cannot be chosen which fits well to all aspects of the feature; we must choose one or the other.
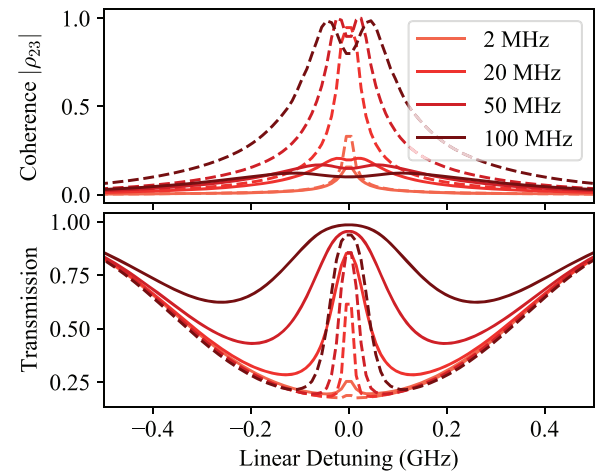
Figure 8. Plot showing the absolute value of the coherence between excited states $|\rho_{23}|$, as extracted from the model, and the corresponding probe transmission. On each plot we compare a closed system (dashed lines), and the open system of our experiment (solid lines), for linear pump Rabi frequencies as shown in the legend.

small sub-features seen in the 0.5 and 1 mW spectra to back reflections, which become more significant at higher powers. Figure 7 shows the experimental trace for 10 μW pump power, plotted with 5.5 MHz and 12.0 MHz model predictions. We see that using this model, we can choose to fit the peak of the absorption window, or the depth of the feature, but not both at once. In our model we assume that the beams have uniform intensity, whereas in reality they have a Gaussian profile; consequently atoms will experience a varying pump intensity as they traverse the beam. The intensity they see is also correlated to the time they spend in the beam. These factors are likely to change the shape of the spectra. For a numerical comparison we use the average Rabi frequency of the beam within the $1/e^2$ waist, and an average power through the cell, taking into account absorption along its length and at cell windows. In this way, 10 μW input power converts to an average Rabi frequency in the cell of 15 MHz, which is close to the two model values. Both the issues mentioned above, and the fact that we do not fully take into account the incomplete spatial overlap of the beams could explain this discrepancy. A more detailed

numerical model beyond the scope of this work is required to fully account for the shape of the EIT features.

7. How significant is the coherent effect?

A relevant question in three-level-systems is whether the spectral features are caused by coherent or incoherent effects [11, 16, 26]. The presence of a prominent enhanced absorption

feature on the transition out of the non-pump-coupled ground state, $|0\rangle$, is evidence that a significant part of the transmission feature does not arise from a coherent EIT effect, but instead from population transfer to a different (and uncoupled) ground state via velocity-selective optical pumping. However, the coherent process is still present, and we can use the model to see this. The density matrix element ρ_{23} is the coherence between $|2\rangle$ and $|3\rangle$, the excited states of our system. Figure 8 compares the transmission (lower panel) and corresponding coherence (upper) for a closed system—meaning no decays into $|0\rangle$—(dotted lines) and our open system (solid lines). A range of pump Rabi frequencies are plotted and coloured according to the legend. We see that as pump Rabi frequency increases, the difference between the coherences in the closed and open systems increases, and that in our system, coherence increases as Rabi frequency increases up to a point (approx. 20 MHz), above which coherence decreases. We also note that for a given pump Rabi frequency the closed system coherence is greater than the open system coherence, while the open system transmission is greater than the closed system transmission. This shows that in our open system the coherence is a small, but present, cause of the feature and that as the pump Rabi frequency increases, its proportional contribution decreases.

8. Conclusions and outlook

In conclusion, we have observed a clean, narrow EIT feature in a V-system and the concomitant enhanced absorption. We see that the EIT feature has contributions from a coherent process, and an incoherent optical pumping process. The incoherent contribution occurs because of the allowed decay from the excited states to both ground states, and is the cause of the enhanced absorption feature. Our theoretical model captures all of the relevant processes, and gives insight into the role of coherence in explaining the observed narrow spectral features. The theoretical treatment is greatly simplified because the experiment was conducted in the hyperfine Paschen-Back regime, leading to distinct non-overlapping resonances.

In this work the Doppler mismatch is small, however the clean system presented here would easily allow investigation of the effect of large mismatches, for example the 5S–5P 5S–6P V-system in rubidium [15, 25], and could be the subject of further study. Another interesting aspect of this work is the sensitivity of the V-EIT spectra to collisional linewidths. Indeed, the study of isolated resonances in the hyperfine Paschen-Back regime could provide a more sensitive spectral measurement of alkali metal–noble gas collisions, and will be the subject of future work.

Disclosures

The authors declare no conflicts of interest.

Data availability statement

The data that support the findings of this study are openly available at the following URL/DOI: doi:10.15128/r2t148fh16h.

ORCID iDs

Clare R Higgins ⓘ https://orcid.org/0000-0002-9835-8478
Ifan G Hughes ⓘ https://orcid.org/0000-0001-6322-6435

References

[1] Arimondo E 1996 V coherent population trapping in laser spectroscopy *Progress in Optics* vol 35 (Amsterdam: Elsevier) pp 257–354
[2] Fleischhauer M, Matsko A B and Scully M O 2000 Quantum limit of optical magnetometry in the presence of ac Stark shifts *Phys. Rev.* A **62** 013808
[3] Budker D and Romalis M 2007 Optical magnetometry *Nat. Phys.* **3** 227–34
[4] Yudin V I, Taichenachev A V, Dudin Y O, Velichansky V L, Zibrov A S and Zibrov S A 2010 Vector magnetometry based on electromagnetically induced transparency in linearly polarized light *Phys. Rev.* A **82** 033807
[5] Hau L V, Harris S E, Dutton Z and Behroozi C H 1999 Light speed reduction to 17 metres per second in an ultracold atomic gas *Nature* **397** 594–8
[6] Das A, Das B C, Bhattacharyya D, Chakrabarti S and De S 2018 Polarization rotation with electromagnetically induced transparency in a V-type configuration of Rb D1 and D2 transitions *J. Phys. B: At. Mol. Opt. Phys.* **51** 175502
[7] Beausoleil R G, Munro W J, Rodrigues D A and Spiller T P 2004 Applications of electromagnetically induced transparency to quantum information processing *J. Mod. Opt.* **51** 2441–8
[8] Hammerer K, Sørensen A S and Polzik E S 2010 Quantum interface between light and atomic ensembles *Rev. Mod. Phys.* **82** 1041–93
[9] Santra R, Arimondo E, Ido T, Greene C H and Ye J 2005 High-accuracy optical clock via three-level coherence in neutral bosonic ^{88}Sr *Phys. Rev. Lett.* **94** 173002
[10] Fleischhauer M, Imamoglu A and Marangos J P 2005 Electromagnetically induced transparency: optics in coherent media *Rev. Mod. Phys.* **77** 633–73
[11] Khan S, Bharti V and Natarajan V 2016 Role of dressed-state interference in electromagnetically induced transparency *Phys. Lett.* A **380** 4100–4
[12] Dey S, Mitra S, Ghosh P N and Ray B 2015 EIT line shape in an open and partially closed multilevel V-type system *Optik* **126** 2711–7
[13] Hazra R and Hossain M M 2020 Study of multi-window electromagnetically induced transparency (EIT) and related dispersive signals in V-type systems in the Zeeman sublevels of hyperfine states of ^{87}Rb-D2 line *J. Phys. B: At. Mol. Opt. Phys.* **53** 235401
[14] Hoshina Y, Hayashi N, Tsubota K, Yoshida I, Shijo K, Sugizono R and Mitsunaga M 2014 Electromagnetically induced transparency in a V-type multilevel system of Na vapor *J. Opt. Soc. Am.* B **31** 1808–13

J. Phys. B: At. Mol. Opt. Phys. **54** (2021) 165403

C R Higgins and I G Hughes

[15] Boon J R, Zekou E, Fulton D J and Dunn M H 1998 Experimental observation of a coherently induced transparency on a blue probe in a Doppler-broadened mismatched V-type system *Phys. Rev.* A **57** 1323–8

[16] Lazoudis A, Kirova T, Ahmed E H, Qi P, Huennekens J and Lyyra A M 2011 Electromagnetically induced transparency in an open V-type molecular system *Phys. Rev.* A **83** 063419

[17] Boon J R, Zekou E, McGloin D and Dunn M H 1999 Comparison of wavelength dependence in cascade-, Λ-, and Vee-type schemes for electromagnetically induced transparency *Phys. Rev.* A **59** 4675–84

[18] Zhu C, Tan C and Huang G 2013 Crossover from electromagnetically induced transparency to Autler–Townes splitting in open V-type molecular systems *Phys. Rev.* A **87** 043813

[19] McGloin D 2003 Coherent effects in a driven Vee scheme *J. Phys. B: At. Mol. Opt. Phys.* **36** 2861–71

[20] Wu Y and Yang X 2005 Electromagnetically induced transparency in V-, Λ-, and cascade-type schemes beyond steady-state analysis *Phys. Rev.* A **71** 053806

[21] Zhao J, Wang L, Xiao L, Zhao Y, Yin W and Jia S 2002 Experimental measurement of absorption and dispersion in V-type cesium atom *Opt. Commun.* **206** 341–5

[22] Scotto S, Ciampini D, Rizzo C and Arimondo E 2015 Four-level N-scheme crossover resonances in Rb saturation spectroscopy in magnetic fields *Phys. Rev.* A **92** 063810

[23] Cha E H, Jeong T and Noh H-R 2014 Two-color polarization spectroscopy in V-type configuration in rubidium *Opt. Commun.* **326** 175–9

[24] Das A, Chandra Das B, Bhattacharyya D and De S 2021 Effects of probe ellipticity and longitudinal magnetic field on the polarization rotation in a coherently prepared atomic medium *OSA Contin.* **4** 105–20

[25] Vdović S, Ban T, Aumiler D and Pichler G 2007 EIT at $5^2S_{1/2} \rightarrow 6^2P_{3/2}$ transition in a mismatched V-type rubidium system *Opt. Commun.* **272** 407–13

[26] Kang H-J and Noh H-R 2017 Coherence effects in electromagnetically induced transparency in V-type systems of ^{87}Rb *Opt. Express* **25** 2176221774

[27] Fulton D J, Shepherd S, Moseley R R, Sinclair B D and Dunn M H 1995 Continuous-wave electromagnetically induced transparency: a comparison of V, Λ, and cascade systems *Phys. Rev.* A **52** 2302–11

[28] Olsen B A, Patton B, Jau Y-Y and Happer W 2011 Optical pumping and spectroscopy of Cs vapor at high magnetic field *Phys. Rev.* A **84** 063410

[29] Weller L, Kleinbach K S, Zentile M A, Knappe S, Adams C S and Hughes I G 2012 Absolute absorption and dispersion of a rubidium vapour in the hyperfine Paschen-Back regime *J. Phys. B: At. Mol. Opt. Phys.* **45** 215005

[30] Zentile M A, Andrews R, Weller L, Knappe S, Adams C S and Hughes I G 2014 The hyperfine Paschen-Back Faraday effect *J. Phys. B: At. Mol. Opt. Phys.* **47** 075005

[31] Ponciano-Ojeda F S, Logue F D and Hughes I G 2020 Absorption spectroscopy and Stokes polarimetry in a ^{87}Rb vapour in the Voigt geometry with a 1.5 T external magnetic field *J. Phys. B: At. Mol. Opt. Phys.* **54** 015401

[32] Sargsyan A, Hakhumyan G, Leroy C, Pashayan-Leroy Y, Papoyan A, Sarkisyan D and Auzinsh M 2014 Hyperfine Paschen-Back regime in alkali metal atoms: consistency of two theoretical considerations and experiment *J. Opt. Soc. Am.* B **31** 1046–53

[33] Sargsyan A, Klinger E, Hakhumyan G, Tonoyan A, Papoyan A, Leroy C and Sarkisyan D 2017 Decoupling of hyperfine structure of Cs D1 line in strong magnetic field studied by selective reflection from a nanocell *J. Opt. Soc. Am.* B **34** 776–84

[34] Ma L, Anderson D A and Raithel G 2017 Paschen-Back effects and Rydberg-state diamagnetism in vapor-cell electromagnetically induced transparency *Phys. Rev.* A **95** 061804

[35] George S, Bruyant N, Béard J, Scotto S, Arimondo E, Battesti R, Ciampini D and Rizzo C 2017 Pulsed high magnetic field measurement with a rubidium vapor sensor *Rev. Sci. Instrum.* **88** 073102

[36] Whiting D J, Keaveney J, Adams C S and Hughes I G 2016 Direct measurement of excited-state dipole matrix elements using electromagnetically induced transparency in the hyperfine Paschen-Back regime *Phys. Rev.* A **93** 043854

[37] Whiting D J, Bimbard E, Keaveney J, Zentile M A, Adams C S and Hughes I G 2015 Electromagnetically induced absorption in a nondegenerate three-level ladder system *Opt. Lett.* **40** 4289–92

[38] Whiting D J, Mathew R S, Keaveney J, Adams C S and Hughes I G 2018 Four-wave mixing in a non-degenerate four-level diamond configuration in the hyperfine Paschen-Back regime *J. Mod. Opt.* **65** 713–22

[39] Whiting D JŠibalić N, Keaveney J, Adams C S and Hughes I G 2017 Single-photon interference due to motion in an atomic collective excitation *Phys. Rev. Lett.* **118** 253601

[40] Adams C S and Hughes I G 2019 *Optics f2f: From Fourier to Fresnel* (Oxford: Oxford University Press)

[41] Harris M L, Adams C S, Cornish S L, McLeod I C, Tarleton E and Hughes I G 2006 Polarization spectroscopy in rubidium and cesium *Phys. Rev.* A **73** 062509

[42] Ro Shin S and Noh H-R 2009 Calculation and measurement of absolute transmission in rubidium *J. Phys. Soc. Japan* **78** 084302

[43] Sagle J, Namiotka R K and Huennekens J 1996 Measurement and modelling of intensity dependent absorption and transit relaxation on the cesium line *J. Phys. B: At. Mol. Opt. Phys.* **29** 2629–43

[44] Hughes I G 2018 Velocity selection in a Doppler-broadened ensemble of atoms interacting with a monochromatic laser beam *J. Mod. Opt.* **65** 640–7

[45] Zentile M A, Keaveney J, Weller L, Whiting D J, Adams C S and Hughes I G 2015 ElecSus: a program to calculate the electric susceptibility of an atomic ensemble *Comput. Phys. Commun.* **189** 162–74